Control Engineering Practice 26 (2014) 1–10

Contents lists available at ScienceDirect

Control Engineering Practice

journal homepage: www.elsevier.com/locate/conengprac

A nonlinear quadrotor trajectory tracking controller with disturbance rejection

David Cabecinhas [a,b,*], Rita Cunha [a], Carlos Silvestre [a,b]

[a] Institute for Robotics and Systems in Engineering and Science (LARSyS), Instituto Superior Técnico, Lisbon, Portugal
[b] Department of Electrical and Computer Engineering, Faculty of Science and Technology, University of Macau, Taipa, Macau, China

ARTICLE INFO

Article history:
Received 10 December 2012
Accepted 30 December 2013
Available online 30 January 2014

Keywords:
Nonlinear control
Trajectory tracking
Disturbance rejection
Backstepping
Quadrotor aircraft

ABSTRACT

This paper addresses the problem of designing and experimentally validating a controller for steering a quadrotor vehicle along a trajectory, while rejecting constant force disturbances. The proposed solution consists of a nonlinear adaptive state feedback controller that asymptotically stabilizes the closed-loop system in the presence of force disturbances. We consider two methods of angular actuation for the quadrotor, angular velocity and torque, and ensure that the actuation does not grow unbounded as a function of the position error. The constant force disturbance is estimated through the use of a sufficiently smooth projector operator. A prototyping and testing architecture, developed to streamline the implementation and the tuning of the controller, is also described. Experimental results are presented to demonstrate the performance and robustness of the proposed controller.

1. Introduction

Flight control and applications of Unmanned Aerial Vehicles (UAV) is an active and challenging topic of research, with crucial importance to numerous civilian and military applications. A great number of recent Journal special issues have been dedicated to these platforms, with topics ranging from the flight control (Fregene & Braatz, 2012) and aerial robotics (Chen, Chen, & Lee, 2011; Hamel, Mahony, & Tayebi, 2010; Michael, Scaramuzza, & Kumar, 2012; Valavanis, 2011) to a plethora of remote sensing applications, like the ones described in detail in Zhou, Ambrosia, Gasiewski, and Bland (2009) and Martinsanz (2012). Vertical take-off and landing (VTOL) rotorcraft, with hover flight capabilities, forms a large and important class of UAVs. From this class, we highlight the quadrotor as an ideal platform for robotic systems, particularly suited for the development and testing of new control strategies due to its simplicity, high maneuverability, and ability to hover.

Flight control is a fundamental problem for quadrotors and aerial vehicles in general. Linear methods have been applied to UAVs with success in Hoffmann, Waslander, and Tomlin (2008), Bouabdallah, Noth, and Siegwart (2004) and more recently Hoffmann, Huang, Waslander, and Tomlin (2011), but are of limited applicability for extended flight envelope regions, i.e. aggressive maneuvers, where the linearity of the system is no longer valid. Additionally, one can only guarantee stability of the closed loop system for small regions around the equilibrium point, which are extremely difficult to compute. Nonlinear controllers based on nested saturations have also been proposed for the tracking of arbitrary trajectories (Naldi, Gentili, Marconi, & Sala, 2010). Due to the nature of the controller, a restriction on the admissible values of the thrust input and on the range of uncertainties of the parameters of the torque generation subsystem is necessary. Additionally, the proposed methodology does not allow for the overturning of the vehicle.

Backstepping is a well known technique extensively used for control of nonlinear systems. For example, it has been applied to helicopter trajectory tracking (Frazzoli, Dahleh, & Feron, 2000; Mahony & Hamel, 2004), to control of a two tilt rotor aircraft (Kendoul, Fantoni, & Lozano, 2006) and also to quadrotor trajectory tracking (Guenard, Hamel, & Mahony, 2008) and tracking of parallel linear visual features (Mahony & Hamel, 2005). In general, the backstepping technique is not applicable to underactuated systems. However, as shown in Koo and Sastry (1998), a simplified model commonly adopted for both quadrotors and helicopters is feedback linearizable by dynamic augmentation of the thrust actuation, and hence stabilizable by means of backstepping. Several methodologies can be combined with backstepping to attain desirable characteristics of a control law, such as robustness to external disturbances and actuation boundedness. The use of integral action to achieve zero steady-state error or equivalently

* Corresponding author at: Department of Electrical and Computer Engineering, Faculty of Science and Technology, Research and Development Building R318, University of Macau, Av. Padre Tomás Pereira, Taipa, Macau, China. Tel: +853 83978550; fax: +853 28838314.
E-mail addresses: dcabecinhas@isr.ist.utl.pt (D. Cabecinhas), rita@isr.ist.utl.pt (R. Cunha), cjs@isr.ist.utl.pt (C. Silvestre).

0967-0661/$ - see front matter © 2014 Elsevier Ltd. All rights reserved.
http://dx.doi.org/10.1016/j.conengprac.2013.12.017

rejection of constant disturbances in a closed-loop regulation system is standard in the control literature and can be combined with the backstepping technique as discussed in Skjetne and Fossen (2004). The control methodology known as adaptive backstepping (Krstic, Kanellakopoulos, & Kokotovic, 1995) relies on an estimator to achieve the disturbance rejection effect of integral control. One problem with a straightforward application of adaptive backstepping is that the parameter estimate can grow, without an *a priori* bound, depending on the initial conditions of the system. The typical approach to this problem is to use a projection operator to constrain the parameter estimate to a given set (Krstic et al., 1995). The discontinuity of the projection operation is a twofold problem. First, it leads to practical problems when applied to continuous time systems. Second, the recursive application of the backstepping procedure is no longer possible, as Lipschitz continuity is violated and the usual theorems on the existence and uniqueness of differentiable equations can no longer be applied. To overcome both these problems, we employ the arbitrarily smooth projection operator proposed in Cai, de Queiroz, and Dawson (2006), which generates parameter estimates with sufficient smoothness to complete the backstepping procedure.

Several works for the stabilization of thrust propelled rotorcraft based on dynamic extension of the thrust input have also been proposed, namely the ones presented in Frazzoli et al. (2000), Mahony and Hamel (2004) and more recently Godbolt and Lynch (2013), Leonard, Martini, and Abba (2012), Kobilarov (2013). Despite employing different control laws, a common characteristic unifies these controllers: the existence of a singularity in the control law for zero thrust. Typically, the singular condition is either ignored or the control laws are modified *ad hoc* when near the singularity, but that leads to a loss of the stability properties and can endanger a vehicle unnecessarily. Nonetheless, for a set of initial error conditions, it can be proven that the thrust never reaches zero and the control law is well defined for all time, as detailed in Mahony and Hamel (2004).

The work in Roberts and Tayebi (2011) employs similar adaptive techniques to achieve control of a VTOL UAV for a set of constant external disturbances. The quadrotor control is constructed by designing a bounded thrust virtual control, which is then tracked using the thrust and torque available controls. The zero thrust singularity is avoided by constraining the virtual control law but that leads to a rather conservative control action. Two controllers are then presented, one which achieves almost global stabilization and other which presents some restrictions on the initial conditions. The estimation and cancelation of the external disturbance is performed using the smooth projection from Cai et al. (2006) to ensure that the estimates are differentiable. As opposed to our method, which treats the rotational degree-of-freedom inherent to these vehicles independently from the position tracking objective, the solution in Roberts and Tayebi (2011) completely prescribes the desired rotation matrix through the attitude extraction method proposed. Simulation results are presented for the proposed controllers, although they are not evaluated in an experimental setup.

Typically, small-scale quadrotors are either controlled in thrust and angular velocity or thrust and torque. With today's technology, there are commonly available sensors for angular velocity with an extremely small footprint that can be carried by even the smallest quadrotor vehicles. This fact makes it easy for aircraft manufacturers to measure the angular velocity and design inner-loop controllers to track angular velocity commands. Torque commands for quadrotor vehicles are also trivial to implement since most electric motors employed in remote controlled aircraft are internally controlled in speed. The motor's angular speed is directly related with the thrust force they generate and by acting on the motors the manufacturer can impose a different force on each motor, so as to track a torque reference.

In this work, we address the problem of trajectory tracking for quadrotors, using a backstepping procedure that builds on the dynamic extension of the thrust input. The desired trajectory is specified by a sufficiently smooth time-parameterized position vector. The desired attitude of the vehicle is not prescribed since attitude convergence (up to a rotation about the body z-axis) is naturally accomplished by solving the position tracking problem. Robustness to external constant disturbances is accomplished through adaptive backstepping. These disturbances can be used to represent both exogenous inputs such as constant wind and model uncertainties such as mass mismatches or uneven mass distribution of the vehicle. The proposed control laws allow us to determine a Lyapunov function for the closed-loop system whose time derivative is negative definite with regard to the tracking errors, rendering it inherently robust to small errors and noise. Experimental results are presented to attest the robustness and performance of the proposed control laws.

A preliminary version of this work was presented in Cunha, Cabecinhas, and Silvestre (2009, 2013). One of the main changes with regard to that preliminary version of this work is the consideration of an external disturbance, modeling the wind force, and its consequent rejection by the proposed control law. The other major improvement is that the control laws for torque actuated vehicles are adapted to quadrotor vehicles actuated in angular velocity and experimentally validated with actual aerial vehicles. Furthermore, the addition of the external disturbance rendered the closed loop systems non-autonomous and lead to a reformulation of the Theorem's proofs by using Barbalat's Lemma.

This paper is structured as follows. Section 2 lays out the mathematical notation used throughout the paper and Section 3 introduces the quadrotor model. The problem and control objectives are stated in Section 4. The controller design is described in Section 5, including the necessary steps to ensure disturbance rejection. Experimental results illustrating the performance of the proposed control law are presented in Sections 6 and 7 draws conclusions from the contents of the paper and points out directions for future work.

2. Notation

Throughout this work we use the prime $f'(x)$ to denote the partial derivative of the function f with respect to x, $f'(x) = (\partial f/\partial x)(x)$, and the upper dot $\dot{f}(x(t)) = f'(x(t))\dot{x}(t)$ to denote the total time derivative of the function. Vectors are represented by bold characters and $\mathbf{e}_1$, $\mathbf{e}_2$, and $\mathbf{e}_3$ denote the unit vectors co-directional with the x-, y-, and z-axis, respectively. When designing an estimator for the unknown quantity x, we use $\hat{x}$ to denote the estimate and $\tilde{x} = x - \hat{x}$ to denote estimation error. A function $\sigma(s) : \mathbb{R} \to \mathbb{R}$ is a *saturation function* if it is differentiable and verifies, for positive M and $\sigma_{\max}$,

$$0 < \sigma'(s) < M \quad \text{for all } s, \tag{1a}$$

$$\sigma(-s) = -\sigma(s) \quad \text{for all } s, \tag{1b}$$

$$s\sigma(s) > 0 \quad \text{for all } s \neq 0, \quad \sigma(0) = 0, \tag{1c}$$

$$\lim_{s \to \pm\infty} \sigma(s) = \pm \sigma_{\max}. \tag{1d}$$

Examples of smooth saturation functions are $\sigma_1(s) = s/\sqrt{1+s^2}$ and $\sigma_2(s) = \arctan(s)$. The map $S(\cdot) : \mathbb{R}^3 \mapsto \mathbb{R}^{3\times 3}$ yields a skew-symmetric matrix that verifies $S(\mathbf{x})\mathbf{y} = \mathbf{x} \times \mathbf{y}$, for $\mathbf{x}$ and $\mathbf{y} \in \mathbb{R}^3$.

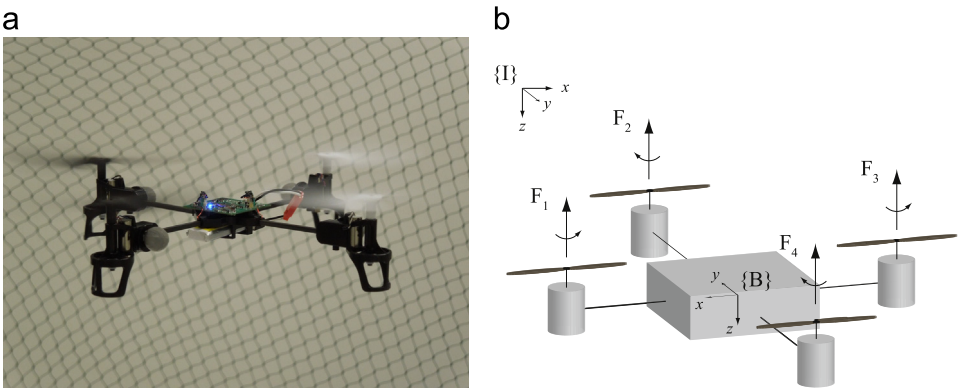

Fig. 1. Quadrotor experimental platform and diagram. (a) Quadrotor platform. (b) Quadrotor setup.

3. Quadrotor model

The quadrotor vehicle is modeled as a rigid body that can generate a thrust force along the body z-axis. We consider two distinct forms of angular actuation: (i) torque, which is equivalent to controlling the force exerted by the electric motors; and (ii) angular velocity. Both are common in quadrotors, whether they are commercial off-the-shelf vehicles or custom built ones.

Consider a fixed inertial frame $\{I\}$ and a frame $\{B\}$ attached to the vehicle's center of mass. The configuration of the body frame $\{B\}$ with respect to $\{I\}$ can be viewed as an element of the Special Euclidean group, $(R, \mathbf{p}) = ({}^I_B R, {}^I\mathbf{p}_B) \in \mathrm{SE}(3)$, where $\mathbf{p} \in \mathbb{R}^3$ is the position and $R \in \mathrm{SO}(3)$ the rotation matrix. The kinematic and dynamic equations of motion for the rigid body can be written as

$$\dot{\mathbf{p}} = R\mathbf{v}, \tag{2a}$$

$$\dot{\mathbf{v}} = -S(\boldsymbol{\omega})\mathbf{v} + \frac{1}{m}\mathbf{f}, \tag{2b}$$

$$\dot{R} = RS(\boldsymbol{\omega}), \tag{2c}$$

$$\dot{\boldsymbol{\omega}} = -\mathbb{J}^{-1}S(\boldsymbol{\omega})\mathbb{J}\boldsymbol{\omega} + \mathbb{J}^{-1}\mathbf{n}, \tag{2d}$$

where the linear velocity $\mathbf{v} \in \mathbb{R}^3$, the force $\mathbf{f} \in \mathbb{R}^3$, the angular velocity $\boldsymbol{\omega} \in \mathbb{R}^3$, and the torque $\mathbf{n} \in \mathbb{R}^3$ are expressed in the body frame $\{B\}$. For quadrotors actuated in angular velocity, only (2a)–(2c) are necessary for a complete model of the vehicle, whereas for actuation in torque the additional angular dynamics (2d) is required. The scalar m and the matrix $\mathbb{J} \in \mathbb{R}^{3\times 3}$ represent the quadrotor's mass and moment of inertia, respectively. For both quadrotor models, the aerodynamic drag forces due to the fuselage are neglected given the low speeds at which the quadrotors operate.

Bearing in mind the geometry of the quadrotor and assuming that the forces and moments generated by each of the four rotors are approximately given by the thrust and torque components perpendicular to the rotor disk plane, we can consider a quadrotor model such that torques (or angular velocities) can be generated in any direction and the generated thrust force is always aligned with the body z-axis. Fig. 1(a) shows a small-scale quadrotor platform and a sketch of the quadrotor setup is presented in Fig. 1(b), together with illustrations of reference frames, the force F_i generated by each motor and the direction of rotation for each propeller. There is a bijective correspondence between the motor forces F_i and the total thrust T and torque $\mathbf{n}$ applied to the quadrotor. We consider that the torque is either an input for the quadrotor or that an inner-loop controller exists that adjusts the torque in order to track angular velocity references. We call this latter design a quadrotor *controlled in angular velocity*.

The total force acting on the quadrotor, in body coordinates, is given by

$$\mathbf{f} = -T\mathbf{e}_3 + mgR^T\mathbf{e}_3 + mR^T\mathbf{b} \tag{3}$$

where T is the thrust generated by the motors, $\mathbf{e}_3 = [0\ 0\ 1]^T$, g is the gravitational acceleration, and $\mathbf{b} \in \mathbb{R}^3$ is an unknown external disturbance expressed in $\{I\}$. The force disturbance $m\mathbf{b}$ can model exogenous inputs, such as constant wind, and also model uncertainties, such as imperfect knowledge of the mass of the vehicle. With the full torque control available, the angular dynamics (2d) can be reduced to the integrator form $\dot{\boldsymbol{\omega}} = \boldsymbol{\tau}$, using the input transformation:

$$\mathbf{n} = \mathbb{J}\boldsymbol{\tau} + S(\boldsymbol{\omega})\mathbb{J}\boldsymbol{\omega}. \tag{4}$$

The quadrotor is thus an underactuated vehicle, as evidenced by (2b) and (3), making the control problem much more difficult to address than what it would be for a fully actuated vehicle. In this particular case we only have one degree of freedom for the force actuation in the body frame and we are required to control the linear position of the vehicle $\mathbf{p} \in \mathbb{R}^3$. It is however possible to control the vehicle's position, as its attitude can be used to drive the thrust force to some desired direction.

4. Problem statement

Let the desired trajectory $\mathbf{p}_d(t) \in \mathbb{R}^3$ be a curve of class at least C^4. The control objective consists of designing a control law for the quadrotor actuations $T(t)$ and $\boldsymbol{\omega}(t)$, or $T(t)$ and $\tau(t)$, that ensures convergence of the vehicle's position $\mathbf{p}(t)$ to the trajectory $\mathbf{p}_d(t)$ with the largest possible basin of attraction. Throughout the remainder of the paper, the time dependence of variables is often omitted to lighten notation.

Due to the underactuated nature of the vehicle, the desired attitude cannot be arbitrarily selected. From (2b) and (3), it is easy to observe that the equilibrium for trajectory tracking satisfies

$$T_d R_d \mathbf{e}_3 = mg\mathbf{e}_3 - m\ddot{\mathbf{p}}_d + m\mathbf{b}. \tag{5}$$

Consequently, the desired rotation matrix R_d is automatically prescribed up to a rotation about the body z-axis ($T_d R_d R_z(\psi)\mathbf{e}_3 = mg\mathbf{e}_3 - m\ddot{\mathbf{p}}_d + m\mathbf{b}$, with $\psi \in \mathbb{R}$). The symmetry exhibited by the quadrotor vehicle dictates that there is an additional degree of freedom. Rotations about the body z-axis bear no influence on the control action as it is possible to generate any angular velocity and thrust, within the vehicle's limits of operation, regardless of its heading angle. Throughout the design of the trajectory tracking controller, the attitude is handled in its natural space, the Special Orthogonal group SO(3), as a rotation matrix. This avoids the introduction of artefacts related only to the parameterization used for the attitude, as is the case of singularities with Euler angles and

multiple coverings with the quaternion representation (Bhat & Bernstein, 2000).

We consider the full state of the vehicle to be available for feedback. In our setup, the state measurements are obtained through a high speed motion tracking system, based on external cameras tracking reflective markers on the vehicle, as described in Section 6.

Although this is hardly ever the case in practice, the external disturbance $\mathbf{b}$ is assumed to be constant for controller design purposes. An upper bound is assumed to be known on the external disturbance, so that the quadrotor can perform a trajectory tracking maneuver with bounded thrust input.

Assumption 1. The external disturbance $\mathbf{b}$ in (3) is constant and is bounded as $\|\mathbf{b}\| \leq B$ with $B > 0$.

In an experimental setup, this is an idealized assumption that approximates reality, thus precluding the attainment of perfect tracking. Nonetheless, the robustness added to the controller by considering constant disturbances is beneficial and results in smaller closed-loop errors.

Even though the disturbance is bounded, straightforward or naive implementations of estimators can lead to wind-up phenomena and result in unbounded growth of the estimate. To avoid a wind-up effect on the disturbance estimator, and keep the estimate bounded, we employ a sufficiently smooth projection operator when designing the estimators. This procedure is detailed in the next section, together with the design of the controller. The smooth projection method requires overparametrization of the disturbance due to the higher order of the quadrotor system. The multiple estimates of the external disturbance, denoted by $\hat{\mathbf{b}}_1$ and $\hat{\mathbf{b}}_2$, are obtained by adaptive backstepping and used for feedback control. Stability of the estimation errors is guaranteed by Lyapunov-like methods from which we can also assert the convergence of the first estimate $\hat{\mathbf{b}}_1$ to the real value of the disturbance, as detailed in the sequel.

5. Controller design

We start the design process by considering a virtual controller for the translational subsystem, which is backstepped through the angular subsystem to obtain the final implementable controllers, one for angular velocity and another for torque actuation. The proposed controller for the translational subsystem is based on the procedure detailed in Mazenc and Iggidr (2004), which is presented in the following proposition for a single double integrator.

Proposition 2. *Consider the double integrator system*

$$\dot{x}_1 = x_2, \tag{6a}$$

$$\dot{x}_2 = u \tag{6b}$$

driven by input $u \in \mathbb{R}$ and let σ, ρ be saturation functions of class C^2 and $\Omega \in C^3$ such that $\Omega(s) = s$, for $|s| < 2\sigma_{\max}$ and $\Omega'(s) \geq 1$ for all s. The control law

$$u(x_1, x_2) = -\frac{(x_2 + \sigma(x_1))(\rho(x_2 + \sigma(x_1)) + \sigma(x_1))}{\Omega'(x_2)(\Omega(x_2) + \Omega(\sigma(x_1)))} + \frac{\sigma'(x_1)x_2}{\Omega'(x_2)} \tag{7}$$

renders the origin of the double integrator globally asymptotically stable and the input verifies

$$|u(x_1, x_2)| \leq \frac{1}{\Omega'(x_2)}(\rho_{\max} + \sigma_{\max} + \sigma'_{\max}|x_2|). \tag{8}$$

Notice that if Ω is, at least, asymptotically quadratic, then an upper bound on $|u(x_1, x_2)|$ can be established *a priori* and for all $(x_1, x_2) \in \mathbb{R}^2$. The Lyapunov function for the double integrator

$$V(x_1, x_2) = \phi(x_1) + \tfrac{1}{2}(\Omega(x_2) + \Omega(\sigma(x_1)))^2, \tag{9}$$

with $\phi(s) = \int_0^s \sigma(t)\, dt$, has closed-loop negative-definite time derivative:

$$\dot{V}(x_1, x_2) = -\sigma(x_1)^2 - (x_2 + \sigma(x_1))\rho(x_2 + \sigma(x_1)). \tag{10}$$

In order to define the virtual controller for the translational subsystem, consider the following error states:

$$\mathbf{z}_1 = \mathbf{p} - \mathbf{p}_d, \tag{11a}$$

$$\mathbf{z}_2 = \dot{\mathbf{z}}_1 + \sigma(\mathbf{z}_1), \tag{11b}$$

for the double integrator driven by

$$\ddot{\mathbf{z}}_1 = \mathbf{u} = -\frac{T}{m}R\mathbf{e}_3 + g\mathbf{e}_3 + \mathbf{b} - \ddot{\mathbf{p}}_d. \tag{12}$$

A tentative Lyapunov function is devised as

$$V_{DI} = \phi(\mathbf{z}_1)^T\mathbf{1} + \tfrac{1}{2}(\Omega(\mathbf{z}_2 - \sigma(\mathbf{z}_1)) + \Omega(\sigma(\mathbf{z}_1)))^T(\Omega(\mathbf{z}_2 - \sigma(\mathbf{z}_1)) + \Omega(\sigma(\mathbf{z}_1))), \tag{13}$$

where, with a slight abuse of notation, ϕ, σ, and Ω are applied element-wise. For a fully actuated vehicle, the control law

$$\mathbf{u}^\star = \begin{bmatrix} u(z_{11}, z_{21} - \sigma(z_{11})) \\ u(z_{12}, z_{22} - \sigma(z_{12})) \\ u(z_{13}, z_{23} - \sigma(z_{13})) \end{bmatrix}, \tag{14}$$

with the controller u defined as in (7), globally asymptotically stabilizes the system and renders the Lyapunov function derivative negative definite:

$$\dot{V}_{DI} = -\sigma(\mathbf{z}_1)^T\sigma(\mathbf{z}_1) - \mathbf{z}_2^T\rho(\mathbf{z}_2) = -W_2(\mathbf{z}_1, \mathbf{z}_2). \tag{15}$$

In the next step, we consider the real vehicle and the errors introduced by the underactuation. Furthermore, a term is added to the Lyapunov function to enable disturbance rejection. The new tentative Lyapunov function is

$$V_2 = V_{DI} + \frac{1}{2k_{b1}}\tilde{\mathbf{b}}_1^T\tilde{\mathbf{b}}_1, \tag{16}$$

with positive gain k_{b1}, and has the following time derivative:

$$\begin{aligned}\dot{V}_2 &= -W_2(\mathbf{z}_1, \mathbf{z}_2) + \frac{\partial V_2}{\partial \mathbf{z}_2}(\mathbf{u} - \mathbf{u}^\star) - \frac{1}{k_{b1}}\tilde{\mathbf{b}}_1^T\dot{\hat{\mathbf{b}}}_1 \\ &= -W_2(\mathbf{z}_1, \mathbf{z}_2) + \frac{\partial V_2}{\partial \mathbf{z}_2}(\hat{\mathbf{u}} - \mathbf{u}^\star) + \tilde{\mathbf{b}}_1^T\left(\frac{\partial V_2}{\partial \mathbf{z}_2}^T - \frac{1}{k_{b1}}\dot{\hat{\mathbf{b}}}_1\right),\end{aligned} \tag{17}$$

where the real control input, computed using the estimated disturbance, is

$$\hat{\mathbf{u}} = -\frac{T}{m}R\mathbf{e}_3 + g\mathbf{e}_3 + \hat{\mathbf{b}}_1 - \ddot{\mathbf{p}}_d \tag{18}$$

and the partial derivative of (16) with respect to $\mathbf{z}_2$ is written as

$$\frac{\partial V_2}{\partial \mathbf{z}_2}^T = (\Omega(\mathbf{z}_2 - \sigma(\mathbf{z}_1)) + \Omega(\sigma(\mathbf{z}_1))) \otimes \Omega'(\mathbf{z}_2 - \sigma(\mathbf{z}_1)) \tag{19}$$

where $\otimes$ denotes element-wise vector multiplication. The term $\hat{\mathbf{u}} - \mathbf{u}^\star$ can be regarded as an actuation error due to the fact that the quadrotor is an underactuated vehicle, i.e. the thrust must be aligned with the z body axis, and due to the unknown disturbance $\mathbf{b}$. Applying the backstepping procedure, we define the new backstepping error:

$$\mathbf{z}_3 = \hat{\mathbf{u}} - \mathbf{u}^\star \tag{20}$$

and the new Lyapunov function:

$$V_3 = V_2 + \tfrac{1}{2}\mathbf{z}_3^T\mathbf{z}_3, \tag{21}$$

with time derivative

$$\dot{V}_3 = -W_3(\mathbf{z}_1,\mathbf{z}_2,\mathbf{z}_3)+\mathbf{z}_3^T\left(k_3\mathbf{z}_3+\frac{\partial V_2}{\partial \mathbf{z}_2}^T+\dot{\mathbf{z}}_3\right)+\tilde{\mathbf{b}}_1^T\left(\frac{\partial V_2}{\partial \mathbf{z}_2}^T-\frac{1}{k_{b1}}\dot{\hat{\mathbf{b}}}_1\right), \tag{22}$$

where $W_3(\mathbf{z}_1,\mathbf{z}_2,\mathbf{z}_3)=W_2+k_3\mathbf{z}_3^T\mathbf{z}_3$ is a positive definite function. The time derivative of the error state $\mathbf{z}_3$ is

$$\dot{\mathbf{z}}_3 = -\frac{\dot{T}}{m}R\mathbf{e}_3-\frac{T}{m}RS(\boldsymbol{\omega})\mathbf{e}_3+\dot{\hat{\mathbf{b}}}_1-\mathbf{p}_d^{(3)}-\dot{\hat{\mathbf{u}}}^\star-\frac{\partial \mathbf{u}^\star}{\partial \mathbf{z}_2}\tilde{\mathbf{b}}_1, \tag{23}$$

where $\dot{\hat{\mathbf{u}}}^\star$ denotes the estimate of the time derivative of $\mathbf{u}^\star$ obtained using $\hat{\mathbf{b}}_1$ instead of the unknown $\mathbf{b}$. The time derivative of the virtual actuation can be expressed as

$$\frac{d\mathbf{u}^\star}{dt}=\frac{\partial \mathbf{u}^\star}{\partial \mathbf{z}_1}\frac{d\mathbf{z}_1}{dt}+\frac{\partial \mathbf{u}^\star}{\partial \mathbf{z}_2}\frac{d\mathbf{z}_2}{dt}, \tag{24}$$

where the external disturbance appearing only linearly in the term $d\mathbf{z}_2/dt$. We have thus that the error when performing the estimation using $\hat{\mathbf{b}}_1$ is given by

$$\dot{\mathbf{u}}^\star-\dot{\hat{\mathbf{u}}}^\star=\frac{\partial \mathbf{u}^\star}{\partial \mathbf{z}_2}\tilde{\mathbf{b}}_1. \tag{25}$$

Substituting $\dot{\mathbf{z}}_3$ in (22) and defining the input vector and matrix,

$$\boldsymbol{\mu}=\begin{bmatrix}\dot{T}\\ \omega_1\\ \omega_2\end{bmatrix},\quad M(T)=\begin{bmatrix}0 & 0 & -T\\ 0 & T & 0\\ -1 & 0 & 0\end{bmatrix},$$

we get an expression for the Lyapunov function time derivative:

$$\dot{V}_3 = -W_3(\mathbf{z}_1,\mathbf{z}_2,\mathbf{z}_3)+\mathbf{z}_3^T\left(\frac{1}{m}RM(T)\boldsymbol{\mu}+k_3\mathbf{z}_3+\frac{\partial V_2}{\partial \mathbf{z}_2}^T+\dot{\hat{\mathbf{b}}}_1-\mathbf{p}_d^{(3)}-\dot{\hat{\mathbf{u}}}^\star\right)$$
$$+\tilde{\mathbf{b}}_1^T\left(\frac{\partial V_2}{\partial \mathbf{z}_2}^T-\frac{\partial \mathbf{u}^{\star T}}{\partial \mathbf{z}_2}\mathbf{z}_3-\frac{1}{k_{b1}}\dot{\hat{\mathbf{b}}}_1\right). \tag{26}$$

We tackle the estimation of the disturbance using a projection operator that keeps the estimate $\hat{\mathbf{b}}_1$ within some *a priori* defined set and verifies the smoothness properties required for the iterative application of the backstepping procedure. Consider the estimate update law

$$\dot{\hat{\mathbf{b}}}_1 = k_{b1}\,\mathrm{Proj}(\xi,\hat{\mathbf{b}}_1)=k_{b1}\left(\xi-\frac{\eta_1\eta_2}{2(\varepsilon^2+2\varepsilon B)^{n+1}B^2}\hat{\mathbf{b}}_1\right) \tag{27}$$

with

$$\xi=\frac{\partial V_2}{\partial \mathbf{z}_2}^T-\frac{\partial \mathbf{u}^{\star T}}{\partial \mathbf{z}_2}\mathbf{z}_3, \tag{28}$$

$$\eta_1=\begin{cases}(\hat{\mathbf{b}}_1^T\hat{\mathbf{b}}_1-B^2)^{n+1} & \text{if } (\hat{\mathbf{b}}_1^T\hat{\mathbf{b}}_1-B^2)>0\\ 0 & \text{otherwise}\end{cases}, \tag{29}$$

$$\eta_2=\hat{\mathbf{b}}_1^T\xi-\sqrt{(\hat{\mathbf{b}}_1^T\xi)^2+\delta^2}, \tag{30}$$

where $\varepsilon>0$ and $\delta>0$ are arbitrary parameters and $B>0$ is the bound on the norm of the unknown parameter. The smooth projection operator is taken from Cai et al. (2006) and has the following properties:

P1 – $\|\hat{\mathbf{b}}(t)\|\le B+\varepsilon,\ \forall t\ge 0$;
P2 – $\tilde{\mathbf{b}}^T\,\mathrm{Proj}(\xi,\hat{\mathbf{b}})\ge\tilde{\mathbf{b}}^T\xi$;
P3 – $\|\mathrm{Proj}(\xi,\hat{\mathbf{b}})\|\le\|\xi\|[1+((B+\varepsilon)/B)]^2+((B+\varepsilon)/(2B^2))\delta$;
P4 – $\mathrm{Proj}(\xi,\hat{\mathbf{b}})$ is C^n.

From the estimator control law (27) and property P2 we derive the upper bound for the Lyapunov function derivative:

$$\dot{V}_3\le -W_3(\mathbf{z}_1,\mathbf{z}_2,\mathbf{z}_3)+\mathbf{z}_3^T\left(\frac{1}{m}RM(T)\boldsymbol{\mu}+k_3\mathbf{z}_3+\frac{\partial V_2}{\partial \mathbf{z}_2}^T+\dot{\hat{\mathbf{b}}}_1-\mathbf{p}_d^{(3)}-\dot{\hat{\mathbf{u}}}^\star\right). \tag{31}$$

Moreover, property P4 ensures that the derivatives of the estimate are continuous up to $\hat{\mathbf{b}}_1^{(n+1)}$. At this time, for vehicles actuated in angular velocity, we can actuate on the control inputs $\boldsymbol{\mu}$ and render (31) negative semi-definite to achieve convergence of the trajectory tracking error to zero. For quadrotors actuated in torque, we need to continue applying the backstepping procedure. Let us look at the Lyapunov derivative upper bound (31) and define the final backstepping error:

$$\mathbf{z}_4=\frac{1}{m}RM(T)\boldsymbol{\mu}+k_3\mathbf{z}_3+\frac{\partial V_2}{\partial \mathbf{z}_2}^T+\dot{\hat{\mathbf{b}}}_1-\mathbf{p}_d^{(3)}-\dot{\hat{\mathbf{u}}}^\star. \tag{32}$$

The error time derivative, finally featuring the torque controls, is

$$\dot{\mathbf{z}}_4=\frac{1}{m}RS(\boldsymbol{\omega})M(T)\boldsymbol{\mu}+\frac{1}{m}R\dot{M}(T)\boldsymbol{\mu}+\frac{1}{m}RM(T)\boldsymbol{\nu}+\dot{\hat{\mathbf{h}}}$$
$$+\frac{\partial}{\partial \mathbf{z}_2}\left(k_3\mathbf{z}_3+\frac{\partial V_2}{\partial \mathbf{z}_2}^T+\dot{\hat{\mathbf{b}}}_1-\mathbf{p}_d^{(3)}-\dot{\hat{\mathbf{u}}}^\star\right)\tilde{\mathbf{b}}_2, \tag{33}$$

where we performed the input transformation

$$\boldsymbol{\nu}=[\ddot{T}\ \ \tau_1\ \ \tau_2]^T \tag{34}$$

and $\hat{\mathbf{h}}$ is the estimate of

$$\mathbf{h}=\frac{d}{dt}\left(k_3\mathbf{z}_3+\frac{\partial V_2}{\partial \mathbf{z}_2}^T+\dot{\hat{\mathbf{b}}}_1-\mathbf{p}_d^{(3)}-\dot{\hat{\mathbf{u}}}^\star\right) \tag{35}$$

obtained using the estimate $\hat{\mathbf{b}}_2$ instead of the unknown disturbance $\mathbf{b}$. The estimation error is given by

$$\mathbf{h}-\hat{\mathbf{h}}=\frac{\partial}{\partial \mathbf{z}_2}\left(k_3\mathbf{z}_3+\frac{\partial V_2}{\partial \mathbf{z}_2}^T+\dot{\hat{\mathbf{b}}}_1-\mathbf{p}_d^{(3)}-\dot{\hat{\mathbf{u}}}^\star\right)\tilde{\mathbf{b}}_2. \tag{36}$$

Let us consider the final Lyapunov function

$$V_4=V_3+\frac{1}{2}\mathbf{z}_4^T\mathbf{z}_4+\frac{1}{2k_{b2}}\tilde{\mathbf{b}}_2^T\tilde{\mathbf{b}}_2 \tag{37}$$

with $k_{b2}>0$ and verify that its time derivative is

$$\dot{V}_4\le -W_4(\mathbf{z}_1,\mathbf{z}_2,\mathbf{z}_3,\mathbf{z}_4)+\mathbf{z}_4^T\left(\mathbf{z}_3+k_4\mathbf{z}_4+\frac{1}{m}RS(\boldsymbol{\omega})M(T)\boldsymbol{\mu}\right.$$
$$\left.+\frac{1}{m}R\dot{M}(T)\boldsymbol{\mu}+\frac{1}{m}RM(T)\boldsymbol{\nu}+\dot{\hat{\mathbf{h}}}\right)$$
$$+\tilde{\mathbf{b}}_2^T\left(\frac{\partial}{\partial \mathbf{z}_2}\left(k_3\mathbf{z}_3+\frac{\partial V_2}{\partial \mathbf{z}_2}^T+\dot{\hat{\mathbf{b}}}_1-\mathbf{p}_d^{(3)}-\dot{\hat{\mathbf{u}}}^\star\right)^T\mathbf{z}_4-\frac{1}{k_{b2}}\dot{\hat{\mathbf{b}}}_2\right). \tag{38}$$

At this point, we can establish a control law for $\boldsymbol{\nu}$ and an estimation law for $\mathbf{b}_2$ that, in conjunction with the previously proposed estimation law (27), renders the Lyapunov function negative semi-definite and achieves trajectory tracking. This result is established in the following theorem.

Theorem 3. *Let the quadrotor kinematics and dynamics be described by (2a)–(2d), let $\mathbf{p}_d(t)\in C^4$ be the reference trajectory, and consider the transformation to error coordinates $\mathbf{z}_1$, $\mathbf{z}_2$, $\mathbf{z}_3$, $\mathbf{z}_4$, given by (11a), (11b), (20), (32), respectively. For any bounded $\tau_3(t)$, the closed-loop system that results from applying the input transformation (34), the control law*

$$\boldsymbol{\nu}=-mM^{-1}(T)R^T\left(\mathbf{z}_3+k_4\mathbf{z}_4+\frac{1}{m}RS(\boldsymbol{\omega})M(T)\boldsymbol{\mu}+\frac{1}{m}R\dot{M}(T)\boldsymbol{\mu}+\dot{\hat{\mathbf{h}}}\right), \tag{39}$$

and the estimator laws (27) and

$$\dot{\hat{\mathbf{b}}}_2=k_b\,\mathrm{Proj}\left(\frac{\partial}{\partial \mathbf{z}_2}\left(k_3\mathbf{z}_3+\frac{\partial V_2}{\partial \mathbf{z}_2}^T+\dot{\hat{\mathbf{b}}}_1-\mathbf{p}_d^{(3)}-\dot{\hat{\mathbf{u}}}^\star\right)^T\mathbf{z}_4,\hat{\mathbf{b}}_2\right), \tag{40}$$

achieves trajectory tracking by guaranteeing that the errors $\mathbf{z}_1, \mathbf{z}_2, \mathbf{z}_3$, *and* $\mathbf{z}_4$ *converge to zero for any initial condition verifying*

$$\sqrt{2V(0)} < g - (B+\varepsilon) - \|\ddot{\mathbf{p}}_d(t)\|_\infty - \mathbf{u}^\star_{\max}, \tag{41}$$

where B is the bound on the external disturbance, $\|\cdot\|_\infty$ *denotes the supremum norm (also called infinity norm) of a function and* $\mathbf{u}^\star_{\max}$ *is the upper bound on the virtual control law* $\mathbf{u}^\star(\mathbf{z}_1, \mathbf{z}_2)$. *Moreover, the disturbance estimate* $\hat{\mathbf{b}}_1$ *converges asymptotically to the unknown constant disturbance* $\mathbf{b}$.

Proof. Starting with the positive definite Lyapunov function,

$$V = \phi(\mathbf{z}_1)^T\mathbf{1} + \frac{1}{2}(\Omega(\mathbf{z}_2 - \sigma(\mathbf{z}_1)) + \Omega(\sigma(\mathbf{z}_1)))^T(\Omega(\mathbf{z}_2 - \sigma(\mathbf{z}_1)) + \Omega(\sigma(\mathbf{z}_1))) + \frac{1}{2}\mathbf{z}_3^T\mathbf{z}_3 + \frac{1}{2}\mathbf{z}_4^T\mathbf{z}_4 + \frac{1}{2k_{b1}}\tilde{\mathbf{b}}_1^T\tilde{\mathbf{b}}_1 + \frac{1}{2k_{b2}}\tilde{\mathbf{b}}_2^T\tilde{\mathbf{b}}_2, \tag{42}$$

and computing its time derivative, in closed-loop, we have that

$$\dot{V} \le -\sigma(\mathbf{z}_1)^T\sigma(\mathbf{z}_1) - k_2\mathbf{z}_2^T\rho(\mathbf{z}_2) - k_3\mathbf{z}_3^T\mathbf{z}_3 - k_4\mathbf{z}_4^T\mathbf{z}_4, \tag{43}$$

which is a negative semi-definite function of the error states and the estimation errors, and is strictly negative definite with regard to the error states. Since the quadrotor error dynamics are non-autonomous, we resort to Barbalat's Lemma to prove convergence of $\dot{V}$ to zero. From the unboundedness of V with respect to the states $\mathbf{z}_1, \mathbf{z}_2, \mathbf{z}_3$, and $\mathbf{z}_4$ and the estimation errors $\tilde{\mathbf{b}}_1$ and $\tilde{\mathbf{b}}_2$, and observing that $\dot{V}$ is negative semi-definite, we conclude that the states, the estimates and estimation errors are bounded. Since $\dot{V}$ is semi-definite negative then the Lyapunov function is upper bounded by $V(0)$ for all time. From that fact and the definition of the error $\mathbf{z}_3$ it follows that $|\mathbf{z}_3| \le \sqrt{2V(0)}$. Observing the bound on error $\mathbf{z}_3$, its definition (20) with (18), and property P1 of the smooth projection operator, we can establish the following conservative lower bound for the thrust input:

$$|T| \ge m(g - (B+\varepsilon) - \|\ddot{\mathbf{p}}_d(t)\|_\infty - \mathbf{u}^\star_{\max} - \sqrt{2V(0)}). \tag{44}$$

The external reference $\mathbf{p}_d$ and its derivatives are bounded by assumption and $\hat{\mathbf{b}}_1$ and $\hat{\mathbf{b}}_2$ are bounded from property P4 of the projection operator and boundedness of the error states and disturbance estimations. From the boundedness of the state $\mathbf{z}_3$, the definitions (18) and (20), and boundedness of the virtual control law (14), $\ddot{\mathbf{p}}$ and estimate $\hat{\mathbf{b}}_1$ we conclude that the thrust force T is bounded. From the definition (32) and boundedness of $\mathbf{z}_4$ we conclude that $\boldsymbol{\mu}$ is bounded if the initial error is within the conditions of the theorem. Finally, boundedness of the time derivative $\dot{\mathbf{z}}_4$ follows from the boundedness of the states, estimates, and the terms in the control law (34). The estimate $\hat{\mathbf{h}}$ and the partial derivatives in (33) are bounded since they are smooth functions of the states and bounded external variables and have no singularities. We have shown that in the conditions of the theorem the control law (39) is well defined and $\ddot{V}$ is bounded from which follows that the time derivative $\dot{V}$ is uniformly continuous. We can therefore apply Barbalat's Lemma to prove convergence of $\dot{V}$ to zero and, consequently, of the error states $\mathbf{z}_1$, $\mathbf{z}_2$, $\mathbf{z}_3$ and $\mathbf{z}_4$ to the origin.

Convergence of the estimate $\hat{\mathbf{b}}_1$ to $\mathbf{b}$ is a consequence of the convergence of the error states to the origin, the definition (20) and the dynamics equation (12). At the error system origin, we have $\mathbf{u}^\star = \mathbf{0}$. From (20) it follows that $\hat{\mathbf{u}} = \mathbf{0}$ and from (12) we get $\mathbf{u} = \mathbf{0}$, leading to the conclusion that the estimate $\hat{\mathbf{b}}_1$ converges to the real external disturbance $\mathbf{b}$.

The rotational degree of freedom allowed for $\omega_3(t)$, or subsequently $\tau_3(t)$, by the term $S(\boldsymbol{\omega})\mathbf{e}_3$ in (23) is due to the axial symmetry exhibited by the quadrotor and can be exploited to control the heading of the vehicle independent of the trajectory tracking law (39). An additional feature of the proposed actuation laws is that they depend only on bounded functions of the position error. This is a desirable property since the initial position error can be arbitrarily large and, without the saturation, would lead to physically infeasible control actuations.

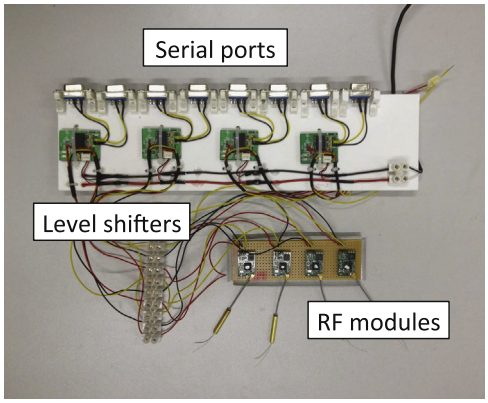

Fig. 2. Serial-port to RF interface used to generate the quadrotor radio control signals from a computer.

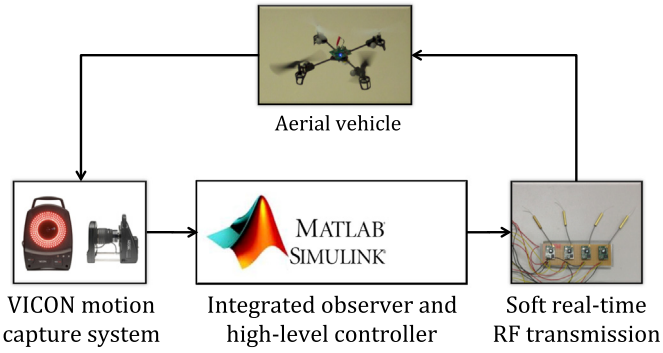

Fig. 3. Quadrotor control architecture.

6. Experimental results

In order to experimentally validate the proposed control algorithms we developed a rapid prototyping and testing architecture using a Matlab/Simulink environment to seamlessly integrate the sensors, the control algorithm, and the communication with the vehicles. The vehicle used for the experiments is a radio controlled Blade mQX quadrotor (Horizon Hobby Inc., 2012), depicted in Fig. 1(a). This aerial vehicle is very agile and maneuverable, readily available and inexpensive, making it the ideal platform for the present work. The quadrotor weighs 80 g with battery included and the arm length from the center of mass to each motor is 11 cm.

Due to the lack of support for on-board sensors, the state of the vehicle must be estimated through external sensors. In our setup we use a VICON Bonita motion capture system (VICON, 2012), comprising 12 cameras, together with markers attached to the quadrotor. The motion capture system is able to accurately locate and estimate the positions of the markers from which it obtains position and orientation measurements for the aircraft. VICON Bonita is a high performance system, able to operate with sub-millimeter accuracy at up to 120 Hz. The performance of the motion capture system is such that the linear velocity can be well estimated from the position measurements by a simple backwards Euler difference, with relatively low noise level. For the experimental setup, the state measurements from the motion capture system are obtained at 50 Hz, allowing for improved accuracy.

The vehicles use a 2.4 GHz wideband Direct Sequence Spread Spectrum signal to generate a robust radio link with on-channel

interference resistance. This radio technology also allows for the simultaneous use of several vehicles in a confined space, enabling formation flight. The commercial off-the-shelf quadrotor vehicles are designed to be human piloted with remote controls but not directly from a computer. In order to be able to send commands to a quadrotor from an external computer we connected the serial interface of the RF module to a computer serial port. Fig. 2 shows four disassembled RF (radio frequency) modules which allow for an extension of the experimental setup to up to four vehicles flying simultaneously. To maintain the radio link, the radio transmitters must receive the control signals via serial port and send them to the vehicle once every 22.5 ms.

A graphical representation of the overall architecture is presented in Fig. 3. We use two computer systems, one running the VICON motion tracking software and the Simulink model which generates the command signals sent to the other computer through Ethernet; and the other that receives the command signals and sends them through serial port to the RF module at intervals of 22.5 ms. The decision to separate control and communications was made to avoid jitter in the transmission of the serial-port signals to the RF module, which occurred when running all the systems in the same computer, and lead to erratic communication with the vehicle.

The Matlab/Simulink interface (see Fig. 4) enables a fast iteration between simulation and experimental testing of control algorithms. A VICON block handles the reception of estimates from the motion capture system and outputs the quadrotor state; computation of the control signals is performed based on measured or simulated vehicle state; and the actuation signals are ultimately relayed to the second computer for radio transmission to the quadrotor or to a simulator block.

6.1. Identification

Identification of the platform was performed by applying different constant commands over several experiments and measuring the thrust force and angular velocity of the vehicle. The thrust force was measured by having weights attached to the quadrotor and finding the thrust command that balanced it. For the angular velocity a command was applied and the angular velocity measured directly with the motion capture system. The radio control system accepts commands in the range $[0, 1]$ for the thrust and $[-1, 1]$ for the angular velocities. The identification results are presented in Fig. 5. The RC commands relate linearly with the vehicle outputs. The maximum thrust generated by the propellers is then approximately 1.37 N (equivalent to 140 g) and varies slightly with the battery charge. Keeping in mind that the commands for angular velocity range between $[-1, 1]$, the maximum angular velocity that can be commanded is 200°/s for the x- and y-axis and 300°/s for the z-axis. However, the commands issued to the quadrotor are not instantaneously followed. This delay nonlinearity can be well approximated by considering the motors as first order dynamic systems with a pole at 1.5 Hz.

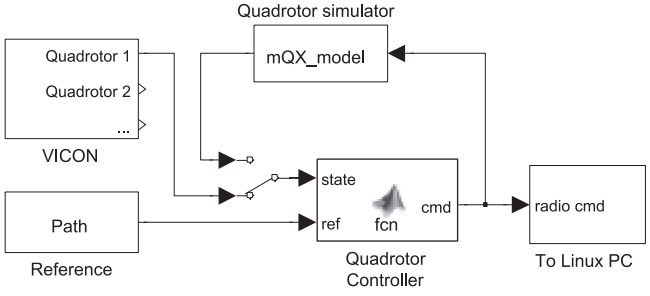

Fig. 4. Simulink block diagram of the quadrotor controller featuring the alternative VICON sensor or quadrotor simulator, reference input, and output to the RF module.

6.2. Trajectory tracking

For the first experimental evaluation of the proposed controller we selected for the desired trajectory a lemniscate (figure eight) parameterized as

$$\mathbf{p}_d(t) = \frac{3}{2} R_x(-\pi/4) R_z(-\pi/6) \begin{bmatrix} \frac{\sin(\phi(t))\cos(\phi(t))}{\sin(\phi(t))^2+1} \\ \frac{\cos(\phi(t))}{\sin(\phi(t))^2+1} \\ 0 \end{bmatrix} + \begin{bmatrix} 0 \\ 0 \\ -1 \end{bmatrix}, \tag{45}$$

where $\phi(t)$ obeys to

$$\dot{\phi}(t) = V\sqrt{1+\sin^2 t}. \tag{46}$$

This parametrization results in a trajectory with unitary norm time derivative and constant desired speed for the quadrotor of V m/s.

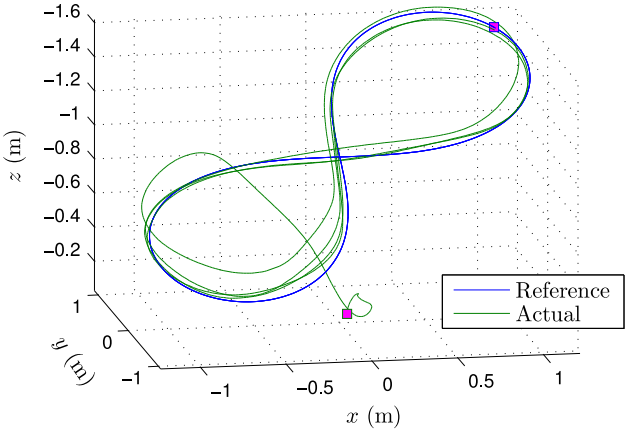

Fig. 6. Comparison of the reference and vehicle trajectories.

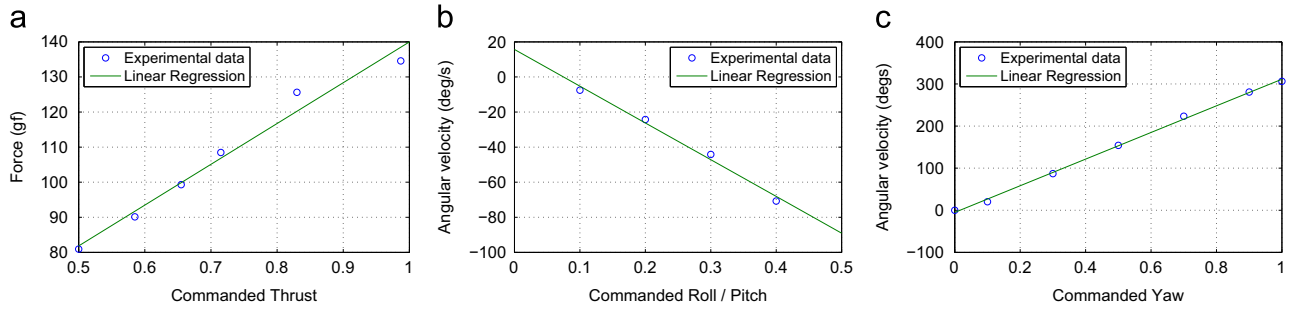

Fig. 5. Quadrotor commands identification. Linear regression of (a) thrust commands, (b) roll/pitch commands, and (c) yaw commands.

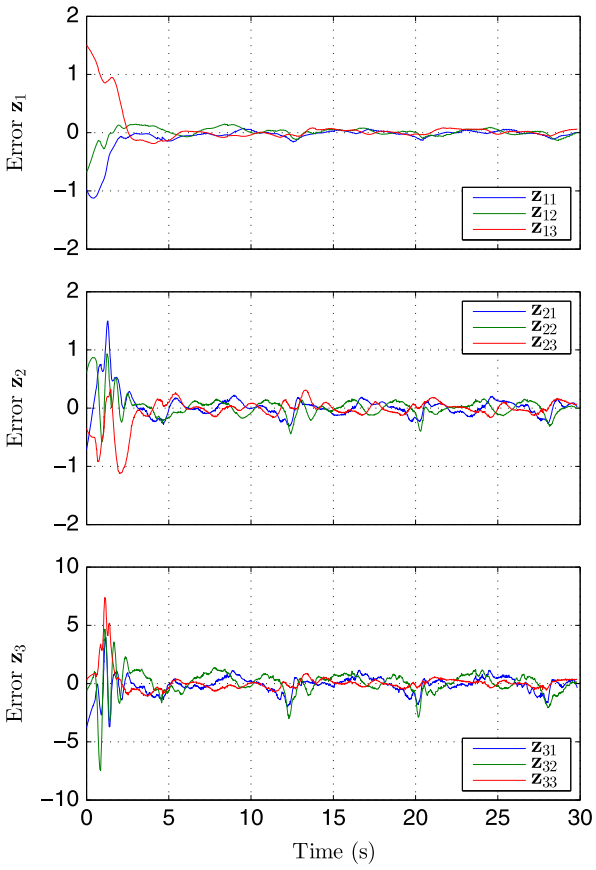

Fig. 7. Time evolution of the error signals.

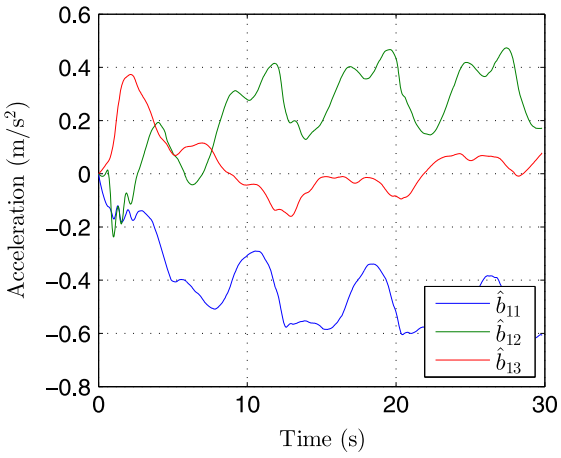

Fig. 8. Disturbance estimate.

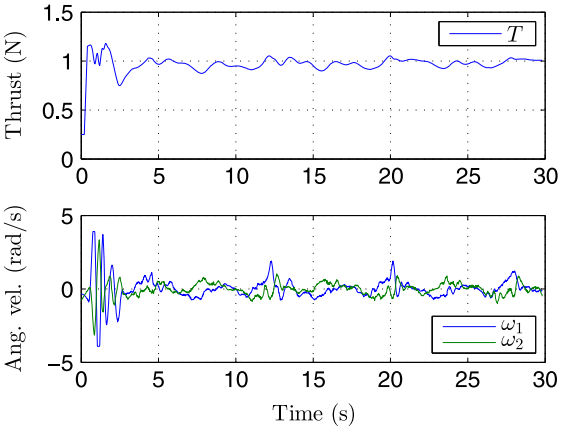

Fig. 9. Time evolution of the actuation signals.

The control law coefficients are $k_3 = 4$, $k_b = 1$, and the initial estimate $\hat{\mathbf{b}}_1(0)$ is set to zero. For the sigmoid function we use

$$\sigma(s) = \frac{Mrs}{\sqrt{1+r^2 s^2}},$$

which has the bound $|\sigma(s)| \leq M$ and derivative at the origin $\sigma'(s) = r$, with $M = 1.5$ and $r = 3$. As yaw input action we use $\omega_3(t) = 0$.

A comparison between the reference trajectory, a lemniscate in an inclined plane described at a speed of $V = 1$ m/s, and the actual quadrotor trajectory is presented in Fig. 6. The quadrotor is initially landed, located approximately at the origin, and the initial reference position is approximately $(1, 1, -1.5)$. Both of these locations are identified by purple markers. The figure shows that the quadrotor trajectory converges to the reference trajectory in a straight fashion, without unnecessary trajectory deviations or changes of direction. After the initial transient, corresponding to the first half of the figure eight, the position error is small, as evidenced by the nearly identical reference and actual lemniscate trajectories.

The quadrotor follows closely the desired path, with negligible position error $\mathbf{z}_1$ in steady state, as can be inferred from the time evolution of the backstepping errors, as shown in Fig. 7. The RMS of the trajectory tracking error $\mathbf{z}_1$ in steady state is 8.5 cm and the maximum error is 16.8 cm. The position error in steady state can be attributed to unmodeled dynamics of the plant and to the fact that the issued commands are not perfectly followed by the aircraft. The main contributions to the unmodeled dynamics are threefold: (i) there exist unmodeled cross-couplings between the angular velocity commands and the lateral forces acting on the quadrotor, due to an uneven and not perfectly symmetric mass distribution of the vehicle; (ii) the issued thrust and angular velocity commands are not perfectly followed due to motor inertia and incorrect thrust command to thrust force identification; (iii) there exist non-constant disturbances affecting the vehicle, mainly due to non-constant wind and a non-constant drag force acting on the quadrotor. Notice that the vehicle has a large initial position error, leading to the saturation function having a preponderant role in the control signal. Despite this unfavorable initial configuration, the actuation commands are kept within their performance limits (see Fig. 9) and convergence to the reference trajectory occurs in just 5 s time, after which only small corrections are performed on the quadrotor trajectory.

Although the trajectory tracking experiment is performed on a closed division, with wind disturbances arising only from an air conditioning system, the effect of the integral action is evidenced on the vertical axis. After the initial transient, where the vertical error decreases rapidly, there is a slower approximation of the altitude to the desired one, until they match in steady state. This slower convergence is the result of the imposed integral action, through the disturbance estimator, which enables perfect theoretical tracking, even though the thrust command to thrust force relation is not perfectly known. The time evolution of the disturbance estimate is presented in Fig. 8. Also visible is the convergence of the estimations of the lateral force errors, on average, to a constant value. These can arise either from uneven mass distribution of the quadrotor or from the fact that the motor and transmission gears have imperfections that result in different rotation velocities, for the same command signal. The estimation does not converge to a constant value but presents some periodic

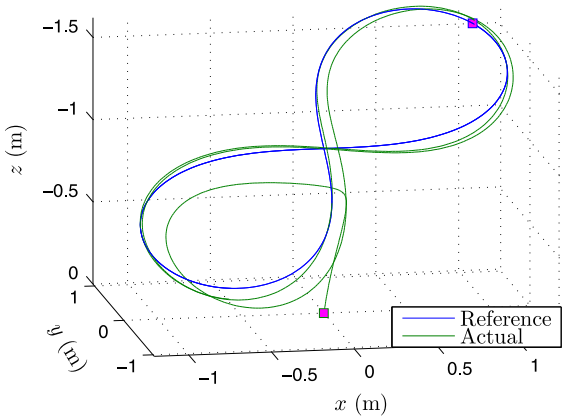

Fig. 10. Comparison of the reference and vehicle trajectories.

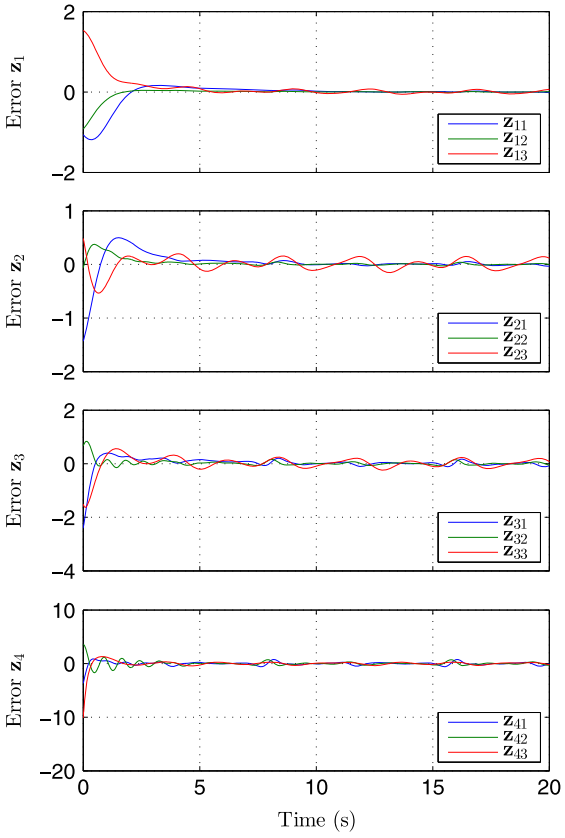

Fig. 11. Time evolution of the error signals.

ripples. The ripples can be explained by the existence of unmodeled dynamics, which disturb the system. The period of the ripples is the same as the period of the trajectory, which is consistent with the unmodeled dynamics hypothesis.

The quadrotor actuation signals are depicted in Fig. 9. The initial transient starts with a high thrust, to take the quadrotor to the desired height, and large angular velocity commands, to turn the quadrotor to the desired direction to minimize the errors. Once in steady state, the actuation signals are primarily the ones necessary to drive the controller through the reference trajectory, with only small corrections being performed according to the control law, without large variations. The thrust actuation is always well above zero and the control law is well defined for all time.

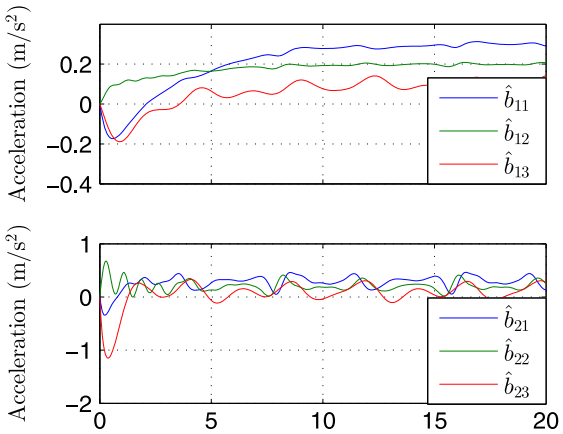

Fig. 12. Disturbance estimate.

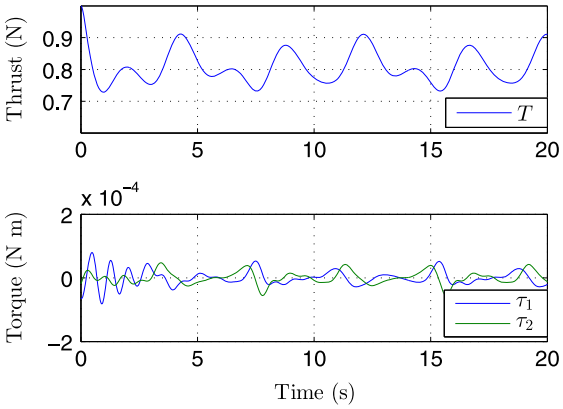

Fig. 13. Time evolution of the actuation signals.

A video of the quadrotor takeoff and trajectory tracking is available at Cabecinhas, Cunha, and Silvestre (2012).

6.3. Torque actuation simulation

We also performed simulation runs of our proposed controller on a quadrotor actuated in torque and thrust. The quadrotor was modeled to be identical to the physical quadrotors available for the experiments. We consider mass $m = 0.080$ kg, an inertia tensor $\mathbb{J} = diag(4.5, 4.5, 9) \times 10^{-4}$ N m, and motors with a pole at 1.5 Hz, which is not taken into account when developing the controller. The control law coefficients are $k_3 = 4$, $k_4 = 5$, $k_{b1} = k_{b2} = 1$, and the initial estimates $\hat{\mathbf{b}}_1(0)$ and $\hat{\mathbf{b}}_2(0)$ are set to zero. A disturbance $\mathbf{b} = [0.3\ 0.2\ 0.1]^T$ was included in the simulation. For the sigmoid functions we use $\sigma(s) = Mrs/\sqrt{1+r^2s^2}$, with $M=1$ and $r=1$ and $\rho(s) = Mrs/\sqrt{1+r^2s^2}$, with $M=1$ and $r=2$. As yaw input action we use $\tau_3(t) = 0$.

Fig. 10 shows a comparison of the reference and actual trajectories. The results are similar to those obtained experimentally, with convergence to the trajectory being attained after one lap around the figure eight, corresponding to around 7 s. Due to the unmodeled vehicle dynamics, resulting from considering the motors as first-order dynamic systems, the trajectory convergence is not perfect. Small residual errors can be observed even in steady state, and are evidenced more clearly in Fig. 11, showing the time evolution of the backstepping errors. Despite the unmodeled dynamics the RMS position error is only 3.4 cm and the maximum error is 7.0 cm.

Observing Fig. 12, one can perceive that the estimate $\hat{\mathbf{b}}_1$ converges to the real value $\mathbf{b}$ and there is not much influence

due to the unmodeled dynamics. The estimate $\hat{\mathbf{b}}_1$ would have converged to the actual disturbance, $\hat{\mathbf{b}}_1 = \mathbf{b}$, in the absence of motor dynamics.

The time evolution of the quadrotor actuation is depicted in Fig. 13. Again, a transient is clearly visible in the first seconds of simulation, where the thrust and torque vary rapidly, until the vehicle is settled close to the desired trajectory. The actuation values for the transient are within the normal values for the steady-state and the singularity $T=0$ is not approached, even during the transient.

7. Conclusions

This paper presented a state feedback solution to the problem of stabilizing an underactuated quadrotor vehicle along a predefined trajectory in the presence of constant force disturbances. A Lyapunov function for the system was derived using adaptive backstepping techniques and made possible by dynamic extension of the actuation. A pair of sufficiently smooth estimators was introduced so as to compensate for the force disturbance and add integral action to the system. Control solutions for different levels of actuation control, which depend on the aircraft, were proposed and tested.

A rapid prototyping and testing architecture was developed to expedite the development process by creating an abstraction layer that integrates the sensors, controller, and communication with the vehicle. Experimental data for trajectory tracking applied to a small-scale quadrotor vehicle was presented which evidenced the effects of the adaptive action and demonstrated the robustness and performance of the proposed control law. Realistic simulation data using a non-ideal torque and thrust actuated quadrotor model was also presented, where the robustness and performance of the proposed controllers with sufficiently smooth estimators were assessed.

The directions of future work are manifold. Foremost, it would be of great utility to extend the basin of attraction of the proposed controller, which for now is restricted to a set of initial conditions for which the tracking error is small. The proposed controller is implementable only in situations where measurements of the full state are available for feedback. This is not a typical circumstance in practice for quadrotors flying outside controlled environments. As such, another promising research direction is the extension of the proposed technique so that only partial state feedback is needed. For the particular case of aerial vehicles, good measurements of the linear velocity are notoriously hard to obtain. A final future research direction can focus on enhancing the trajectory tracking control law so that the inherent limitations of the actuators are always respected, independent of the trajectory to be tracked and initial state of the vehicle.

Acknowledgments

The authors are grateful to Bruno Cardeira for his contributions to the construction of the experimental setup and the communication interface with the vehicle. This work was partially supported by project FCT PEst-OE/EEI/LA0009/2013 and by project FCT SCARVE (PTDC/EEA-CRO/102857/2008). The work of D. Cabecinhas was supported by the FCT Doctoral Grant from the FCT POCTI program, SFRH/BD/31439/2006.

References

Bhat, S. P., & Bernstein, D. S. (2000). A topological obstruction to continuous global stabilization of rotational motion and the unwinding phenomenon. *Systems and Control Letters*, *39*, 63–70.

Bouabdallah, S., Noth, A., & Siegwart, R. (2004). PID vs LQ control techniques applied to an indoor micro quadrotor. In *Proceedings of the international conference on intelligent robots and systems* (pp. 2451–2456).

Cabecinhas, D., Cunha, R., & Silvestre, C. (2012). Video of the trajectory tracking experimental results. URL: ⟨http://users.isr.ist.utl.pt/~dcabecinhas/CEPtrajtrack.m4v⟩.

Cai, Z., de Queiroz, M., & Dawson, D. (2006). A sufficiently smooth projection operator. *IEEE Transactions on Automatic Control*, *51*, 135–139.

Chen, C., Chen, B. M., Lee, & T. H. (Eds.). (2011). Development of autonomous unmanned aerial vehicles [Special issue]. *Mechatronics*, *21*.

Cunha, R., Cabecinhas, D., & Silvestre, C. (2009). Nonlinear trajectory tracking control of a quadrotor vehicle. In *Proceedings of the European control conference*.

Cunha, R., Cabecinhas, D., & Silvestre, C. (2013). Experimental evaluation of a backstepping controller for a quadrotor with wind disturbance rejection. In *Proceedings of the European control conference*.

Frazzoli, E., Dahleh, M., & Feron, E. (2000). Trajectory tracking control design for autonomous helicopters using a backstepping algorithm. In *Proceedings of the American control conference* (pp. 4102–4107).

Fregene, K., & Braatz, R. D. (Eds.). (2012). Unmanned aerial vehicle [Special issue]. *IEEE Control Systems*, *32*.

Godbolt, B., & Lynch, A. F. (2013). Model-based helicopter UAV control: Experimental results. *Journal of Intelligent & Robotic Systems*, 1–13, http://dx.doi.org/10.1007/s10846-013-9898-3.

Guenard, N., Hamel, T., & Mahony, R. (2008). A practical visual servo control for an unmanned aerial vehicle. *IEEE Transactions on Robotics*, *24*, 331–340.

Hamel, T., Mahony, R., & Tayebi, A. (Eds.). (2010). Aerial robotics [Special issue]. *Control Engineering Practice*, *18*, 677–836.

Hoffmann, G. M., Huang, H., Waslander, S. L., & Tomlin, C. J. (2011). Precision flight control for a multi-vehicle quadrotor helicopter testbed. *Control Engineering Practice*, *19*, 1023–1036.

Hoffmann, G. M., Waslander, S. L., & Tomlin, C. J. (2008). Quadrotor helicopter trajectory tracking control. In *Proceedings of the AIAA guidance, navigation, and control conference*.

Horizon Hobby Inc. (2012). Blade mqx ultra micro quad-copter. URL: ⟨http://www.bladehelis.com/Products/Default.aspx?ProdID=BLH7500⟩.

Kendoul, F., Fantoni, I., & Lozano, R. (2006). Modeling and control of a small autonomous aircraft having two tilting rotors. *IEEE Transactions on Robotics*, *22*, 1297–1302.

Kobilarov, M. (2013). Trajectory tracking of a class of underactuated systems with external disturbances. In *Proceedings of the American control conference* (pp. 1044–1049).

Koo, T. J., & Sastry, S. (1998). Output tracking control design of a helicopter model based on approximate linearization. In *Proceedings of the IEEE conference on decision and control* (pp. 3635–3640).

Krstic, M., Kanellakopoulos, I., & Kokotovic, P. V. (1995). *Nonlinear and adaptive control design*. Wiley, New York.

Leonard, F., Martini, A., & Abba, G. (2012). Robust nonlinear controls of model-scale helicopters under lateral and vertical wind gusts. *IEEE Transactions on Control Systems Technology*, *20*, 154–163.

Mahony, R., & Hamel, T. (2004). Robust trajectory tracking for a scale model autonomous helicopter. *International Journal of Robust and Nonlinear Control*, *14*, 1035–1059.

Mahony, R., & Hamel, T. (2005). Image-based visual servo control of aerial robotic systems using linear image features. *IEEE Transactions on Robotics*, *21*, 227–239.

Martinsanz, G. P. (Ed.). (2012). Unmanned aerial vehicles (UAVS) based remote sensing [Special issue]. *Remote Sensing*, *4*.

Mazenc, F., & Iggidr, A. (2004). Backstepping with bounded feedbacks. *Systems & Control Letters*, *51*, 235–245.

Michael, N., Scaramuzza, D., & Kumar, V. (Eds.). (2012). Micro-UAV perception and control [Special issue]. *Autonomous Robots*, *33*.

Naldi, R., Gentili, L., Marconi, L., & Sala, A. (2010). Design and experimental validation of a nonlinear control law for a ducted-fan miniature aerial vehicle. *Control Engineering Practice*, *18*, 747–760.

Roberts, A., & Tayebi, A. (2011). Adaptive position tracking of VTOL UAVs. *IEEE Transactions on Robotics*, *27*, 129–142.

Skjetne, R., & Fossen, T. (2004). On integral control in backstepping: Analysis of different techniques. In *Proceedings of the American control conference* (pp. 1899–1904).

Valavanis, K. (Ed.). (2011). Unmanned aerial vehicles [Special issue]. *Journal of Intelligent and Robotic Systems*, *61*.

VICON. (2012). Motion capture systems from vicon. URL: ⟨http://www.vicon.com⟩.

Zhou, G., Ambrosia, V., Gasiewski, A. J., & Bland, G. (Eds.). (2009). Unmanned airborne vehicle (UAV) sensing systems for earth observations [Special issue]. *IEEE Transactions on Geoscience and Remote Sensing*, *47*.